Research Article | Vol. 26, No. 2 | 22 Jan 2018 | OPTICS EXPRESS 2132
Optics EXPRESS

Estimation of fluorescent Donaldson matrices using a spectral imaging system

SHOJI TOMINAGA,[1,2,*] KEITA HIRAI,[1] AND TAKAHIKO HORIUCHI[1]

[1]*Department of Imaging Sciences, Graduate School of Engineering, Chiba University, 1-33 Yayoi-cho, Inage-ku, Chiba, 263-8522, Japan*
[2]*Department of Computer Science, Norwegian University of Science and Technology, Teknologivegen 22, 2815 Gjøvik, Norway*
**shojitominaga12@gmail.com*

Abstract: The present paper proposes a method to estimate the bispectral Donaldson matrices of fluorescent objects in a scene with a spectral imaging system. Multiple ordinary light sources with continuous spectral-power distributions are projected sequentially onto object surfaces without controlling the spectral shape of the illumination source. The estimation problem of the Donaldson matrices is solved as an optimization problem, where the residual error of observations by the spectral imaging system is minimized. The reflection, emission, and excitation spectral functions are estimated at each wavelength without using a basis function approximation. To improve the estimation efficiency, the output visible range is segmented into two types of wavelength ranges: one for only reflection and another for both reflection and emission. An iterative algorithm is then developed based on the wavelength segmentation and the physical excitation model. The usefulness of the proposed method is examined in experiments using different fluorescent objects and illuminants. We show the estimation accuracy of the Donaldson matrices, discuss the effective selection of illuminants, and demonstrate an application to spectral analysis and reconstruction of a fluorescent image.

OCIS codes: (110.0110) Imaging systems; (110.4234) Multispectral and hyperspectral imaging.

References and links

1. R. Donaldson, "Spectrophotometry of fluorescent pigments," Br. J. Appl. Phys. **5**(6), 210–214 (1954).
2. D. Gundlach and H. Terstiege, "Problems in measurement of fluorescent materials," Color Res. Appl. **19**(6), 427–436 (1994).
3. CIE, "Calibration methods and photo-luminescent standards for total radiance factor measurements," CIE 182:2007, Commission Internationale de l'Eclairage, Vienna (2007).
4. E. Fuchs, "Separating the fluorescence and reflectance components of coral spectra," Appl. Opt. **40**(21), 3614–3621 (2001).
5. A. Lam and I. Sato, "Spectral modeling and relighting of reflective-fluorescent scenes," in *Proceedings of IEEE Conference on Computer Vision and Pattern Recognition* (IEEE, 2013), pp. 1452–1459.
6. Y. Zheng, Y. Fu, A. Lam, I. Sato, and Y. Sato, "Separating fluorescent and reflective components by using a single hyperspectral image," in *Proceedings of IEEE International Conference on Computer Vision* (IEEE, 2015), pp. 3523–3531.
7. Y. Fu, A. Lam, I. Sato, T. Okabe, and Y. Sato, "Separating reflective and fluorescent components using high frequency illumination in the spectral domain," IEEE Trans. Pattern Anal. Mach. Intell. **38**(5), 965–978 (2016).
8. Y. Fu, A. Lam, Y. Kobayashi, I. Sato, T. Okabe, and Y. Sato, "Reflectance and fluorescent spectra recovery based on fluorescent chromaticity invariance under varying illumination," in *Proceedings of IEEE Conference on Computer Vision and Pattern Recognition* (IEEE, 2014), pp. 2171–2178.
9. H. Blasinski, J. Farrell, and B. Wandell, "Simultaneous surface reflectance and fluorescence spectra estimation," arXiv:1605.04243 (2016).
10. J. Suo, L. Bian, F. Chen, and Q. Dai, "Bispectral coding: compressive and high-quality acquisition of fluorescence and reflectance," Opt. Express **22**(2), 1697–1712 (2014).
11. S. Tominaga, K. Hirai, and T. Horiuchi, "Estimation of bispectral Donaldson matrices of fluorescent objects by using two illuminant projections," J. Opt. Soc. Am. A **32**(6), 1068–1078 (2015).
12. S. Tominaga, K. Kato, K. Hirai, and T. Horiuchi, "Spectral image analysis of mutual illumination between florescent objects," J. Opt. Soc. Am. A **33**(8), 1476–1487 (2016).
13. S. Tominaga, K. Kato, K. Hirai, and T. Horiuchi, "Spectral image analysis and appearance reconstruction of fluorescent objects under different illuminations," in *Proceedings of 4th CIE Expert Symposium on Colour and Visual Appearance* (CIE, 2016), pp. 140–146.

#312990 https://doi.org/10.1364/OE.26.002132
Journal © 2018 Received 8 Nov 2017; revised 12 Jan 2018; accepted 14 Jan 2018; published 19 Jan 2018

Optics EXPRESS

14. S. Tominaga, K. Kato, K. Hirai, and T. Horiuchi, "Appearance decomposition and reconstruction of textured fluorescent objects," in *Proceedings of IS&T Inter. Sympo. Electronic Imaging 2017 in the Material Appearance Conference* (IS&T, 2017), pp. 42–47.
15. M. Mohammadi, Developing an Imaging Bi-Spectrometer for Fluorescent Materials, Ph.D. Dissertation, Chester F. Carlson Center for Imaging Science, RIT (2009).
16. F. Schieber, "Modeling the Appearance of Fluorescent Colors," in *Proceedings of Human Factors and Ergonomics Society Annual Meeting* (SAGE, 2001), pp. 1324–1327.
17. J. R. Lakowicz, *Principles of Fluorescence Spectroscopy*, 3rd ed. (Springer, 2006).
18. M. S. Wrighton, D. S. Ginley, and D. L. Morse, "A technique for the determination of absolute emission quantum yields of powdered samples," J. Phys. Chem. **78**(22), 2229–2233 (1974).
19. H. Ishida, S. Tobita, Y. Hasegawa, R. Katoh, and K. Nozaki, "Recent advances in instrumentation for absolute emission quantum yield," Coord. Chem. Rev. **254**(21–22), 2449–2458 (2010).
20. B. A. Hullin, J. Hanika, B. Ajdin, H. P. Seidel, J. Kautz, and H. P. A. Lensch, "Acquisition and analysis of bispectral bidirectional reflectance and reradiation distribution functions," ACM Trans. Graph. **29**(4), 97 (2010).
21. O. Shimomura, "Discovery of green fluorescent protein (GFP) (Nobel Lecture)," Angew. Chem. Int. Ed. Engl. **48**(31), 5590–5602 (2009).
22. E. H. Murchie and T. Lawson, "Chlorophyll fluorescence analysis: a guide to good practice and understanding some new applications," J. Exp. Bot. **64**(13), 3983–3998 (2013).
23. S. Lenk, L. Chaerle, E. E. Pfündel, G. Langsdorf, D. Hagenbeek, H. K. Lichtenthaler, D. Van Der Straeten, and C. Buschmann, "Multispectral fluorescence and reflectance imaging at the leaf level and its possible applications," J. Exp. Bot. **58**(4), 807–814 (2007).
24. S. Delalieux, A. Auwerkerken, W. W. Verstraeten, B. Somers, R. Valcke, S. Lhermitte, J. Keulemans, and P. Coppin, "Hyperspectral reflectance and fluorescence imaging to detect scab induced stress in apple leaves," Remote Sens. **1**(4), 858–874 (2009).
25. P. L. Choyke and H. Kobayashi, "Medical uses of fluorescence imaging: Bringing disease to light," IEEE J. Sel. Top. Quantum Electron. **18**(3), 1140–1146 (2012).
26. E. G. Borisova, L. P. Angelova, and E. P. Pavlova, "Endogenous and exogenous fluorescence skin cancer diagnostics for clinical applications," IEEE J. Sel. Top. Quantum Electron. **20**(2), 211–222 (2014).
27. K. Nishino, K. Nakamura, M. Tsuta, M. Yoshimura, J. Sugiyama, and S. Nakauchi, "Optimization of excitation-emission band-pass filter for visualization of viable bacteria distribution on the surface of pork meat," Opt. Express **21**(10), 12579–12591 (2013).
28. J. Horigome, M. Kozuma, and T. Shirasaki, "Fluorescence pattern analysis to assist food safety -Food analysis technology driven by fluorescence fingerprints-," Hitachi Review **65**(7), 248–254 (2016).
29. S. Gonzalez and M. D. Fairchild, "Evaluation of bispectral spectrophotometry for accurate colorimetry of printing materials," in *Proceedings of Color Imaging Conference* (IS&T, 2000), pp. 39–43.
30. L. G. Coppel, M. Andersson, O. Norberg, and S. Lindberg, "Impact of illumination spectral power distribution on radiance factor of fluorescing materials," in *Proceedings of Colour and Visual Computing Symposium* (IEEE, 2013), pp. 1–4.
31. C. A. Stedmon, S. Markager, and R. Bro, "Tracing dissolved organic matter in aquatic environments using a new approach to fluorescence spectroscopy," Mar. Chem. **82**(3–4), 239–254 (2003).

1. Introduction

Over the years, the use of fluorescent materials has increased in our daily lives. All kinds of everyday objects are made of such materials, including paint, dye, paper, plastic, and cloth. The usefulness of fluorescence is based on the effect that the visual appearance of the object surface is improved compared to a reflective surface based on non-fluorescent reflection. Because of fluorescent emissions, many fluorescent surfaces appear brighter and more vivid with respect to the original color of the surface.

The fluorescent characteristics are well-described in terms of their bispectral radiance factor. The radiance factor is a function of two wavelength variables: the excitation wavelength of incident light and the emission/reflection wavelength. The bispectral radiance factor can be summarized as a Donaldson matrix [1], which is an illuminant independent matrix representing the bispectral radiance factor of a target object. The bispectral radiance factor can be measured using two monochromators [2, 3]. However, the two-monochromator method is time-consuming and expensive. Thus, its use is confined to the laboratory and it is not available in ordinary imaging systems.

Although there have been many papers related to reflectance and fluorescent spectral recovery using an imaging system, most of them do not consider estimation of the Donaldson matrix. Rather, they separate fluorescent emission and reflectance (e.g., see [4–7]). Some

Optics EXPRESS

approaches towards Donaldson matrix estimation are found in a limited number of papers [8–11].

It is usually considered that control of the illuminant spectrum is required in order to distinguish the reflected and luminescent photons. For example, Fu et al. [8] described a method that uses nine colored light in the visible range (400 to 700 nm) to recover the reflectance spectrum and the relative spectrum of emission and absorption from color camera data. Blasinski et al. [9] presented a framework that can estimate the reflectance spectrum and the absolute emission and absorption spectra in two fluorophores. This method is based on an imaging system consisting of many narrowband light sources and transmission filters attached to a camera. These methods used a linear basis function approximation to represent three spectral functions of reflectance, emission, and excitation. However, the selection of basis functions is not easy because the three spectral functions have unique spectral features. Increasing the number of basis functions may lead to an improvement of the spectral approximation, but that will result in an increased number of narrowband light sources. It should be noted that increasing the number of unknown parameters does not result in reliable spectral estimation. The optimal selection of basis functions, illuminant spectrum, and camera filtration is still a problem. Suo et al. [10] described an imaging system that uses programmable spectral filters placed in both sides of light source and camera. Although this approach could yield a direct estimation of the Donaldson matrix, the spectral sampling was too rough to use in practical fluorescent analysis.

Tominaga et al. [11] presented an approach using a spectral imaging system where only two illuminants with different spectra are projected onto an object without controlling the spectral shapes. The Donaldson matrix was modeled with high spectral resolution. This had the possibility to be used for several fluorescence analyses, such as mutual illumination [12], appearance reconstruction [13], and texture analysis [14]. The principle of the Donaldson matrix estimation was based on that the difference between the total radiance factors observed under the two illuminants. This difference was caused only by the luminescent radiance component due to fluorescent emission. However, the method was a graphical approach for finding spectral differences between the two total spectral radiance factors. Thus, the estimation results were often unreliable and unstable, especially for low intensity light sources.

The present paper proposes a stable and reliable method to estimate the bispectral Donaldson matrices for spectral imaging data of fluorescent objects. We suppose a general image acquisition system that allows more than two illuminant projections. The Donaldson matrix is modeled as a 71×60 array in spectrally high dimension. Excitation is defined in a 350 to 700 nm wavelength range, and emission range is defined a 400 to 700 nm wavelength range.

The estimation problem is solved as an optimization problem, where the residual error of the observations acquired by the spectral imaging system is minimized. We estimate the spectral functions of reflectance, emission, and excitation in a direct way without using basis functions. The output visible wavelength is segmented into two types of wavelength ranges: one consisting of only reflection and another consisting of both reflection and emission. In the first range, the reflectance is straightforward estimated; in the second range, the reflection and emission spectra are estimated iteratively. The excitation spectrum is estimated using a physical model. The emission wavelength range is determined based on error minimization. The usefulness of the proposed method is examined in experiments using different fluorescent objects and illuminants. We show how precisely the algorithm estimates the Donaldson matrix of a fluorescent object with a fluorophore. The effective selection of illuminants is discussed with the presented experiments. Finally, a successful application to spectral analysis and reconstruction of a fluorescent image is demonstrated using a real scene, which includes different fluorescent and non-fluorescent materials.

Optics EXPRESS

2. Bispectral modeling

2.1 Donaldson matrix for a fluorescent object

A Donaldson matrix $D(\lambda_{em},\lambda_{ex})$ represents the bispectral radiance factor of a fluorescent object as a two-variable function of the excitation wavelength λ_{em} and the emission/reflection wavelength λ_{ex}. The excitation wavelength range for all fluorescent materials starts from about 330 to 350 nm (see [15,16]). Because most light sources used in everyday life contain some ultraviolet (UV) component that contributes to fluorescent emission, the excitation range in this paper is set to $350 \le \lambda_{ex} \le 700$ nm. As our spectral imaging system operates in the visible wavelength range, the emission/reflection range is set to $400 \le \lambda_{em} \le 700$ nm.

The Donaldson matrix is decomposed into two components of the reflected radiance factor $D_R(\lambda_{em},\lambda_{ex})$ by light reflection, and the luminescent radiance factor $D_L(\lambda_{em},\lambda_{ex})$ by fluorescent emission. The matrix $D_R(\lambda_{em},\lambda_{ex})$ is diagonal and has values only at $\lambda_{em}=\lambda_{ex}$. This corresponds to surface spectral reflectance $S(\lambda)$ because monochrome light reflected from a surface has the same wavelength as the incident light. The matrix $D_L(\lambda_{em},\lambda_{ex})$ has values only in the off-diagonal of satisfying $\lambda_{em}>\lambda_{ex}$ because the luminescent energy is emitted at a longer wavelength than each excitation wavelength due to the Stokes shift [17]. In this study, the luminescent radiance factor is separated into a multiplication of excitation and emission wavelength components as $D_L(\lambda_{em},\lambda_{ex})=\alpha(\lambda_{em})\beta(\lambda_{ex})$. The two functions $\alpha(\lambda_{em})$ and $\beta(\lambda_{ex})$ are the emission and excitation spectra, respectively. The chromaticity invariance of fluorescence emission [8, 9, 11] is derived from this separation property. The above multiplication of $\alpha(\lambda_{em})$ and $\beta(\lambda_{ex})$ implies that one of two spectra can be arbitrarily rescaled. Therefore, we assume that the excitation spectrum is normalized such that $\int_{350}^{700}\beta(\lambda_{ex})d\lambda_{ex}=1$.

A discrete form of the Donaldson matrix with the above properties can be represented in an $N\times M$ matrix as

$$\begin{aligned}\mathbf{D}&=\mathbf{D}_{\mathrm{R}}+\mathbf{D}_{\mathrm{L}}\\&=\begin{bmatrix}0&\cdots&0&s_1&0&\cdots&0\\0&&0&0&s_2&\ddots&\vdots\\\vdots&&\vdots&\vdots&\ddots&\ddots&0\\0&\cdots&0&0&\cdots&0&s_N\end{bmatrix}+\begin{bmatrix}\alpha_1\beta_1&\cdots&\alpha_1\beta_{M-N}&0&0&\cdots&0\\\alpha_2\beta_1&&\alpha_2\beta_{M-N}&\alpha_2\beta_{M-N+1}&0&\ddots&\vdots\\\vdots&&\vdots&\vdots&\ddots&\ddots&0\\\alpha_N\beta_1&\cdots&\alpha_N\beta_{M-N}&\alpha_N\beta_{M-N+1}&\cdots&\alpha_N\beta_{M-1}&0\end{bmatrix}\\&=\begin{bmatrix}\alpha_1\beta_1&\cdots&\alpha_1\beta_{M-N}&s_1&0&\cdots&0\\\alpha_2\beta_1&&\alpha_2\beta_{M-N}&\alpha_2\beta_{M-N+1}&s_2&\ddots&\vdots\\\vdots&&\vdots&\vdots&\ddots&\ddots&0\\\alpha_N\beta_1&\cdots&\alpha_N\beta_{M-N}&\alpha_N\beta_{M-N+1}&\cdots&\alpha_N\beta_{M-1}&s_N\end{bmatrix},\end{aligned}\quad(1)$$

where s_i (i = 1, 2, .., N), α_i (i = 1, 2, .., N), and β_i (i = 1, 2, .., M-1) represent the discrete reflectance, emission, and excitation spectra, respectively. When the spectral functions are sampled in equal 5 nm wavelength intervals, the Donaldson matrix is rewritten with M = 71 and N = 61 as follows:

Optics EXPRESS

$$\mathbf{D}=\begin{bmatrix} \alpha_1\beta_1 & \cdots & \alpha_1\beta_{10} & s_1 & 0 & \cdots & 0 \\ \alpha_2\beta_1 & & \alpha_2\beta_{10} & \alpha_2\beta_{11} & s_2 & \ddots & \vdots \\ \vdots & & \vdots & \vdots & \ddots & \ddots & 0 \\ \alpha_{61}\beta_1 & \cdots & \alpha_{61}\beta_{10} & \alpha_{61}\beta_{11} & \cdots & \alpha_{61}\beta_{70} & s_{61} \end{bmatrix} \tag{2}$$

Figure 1 demonstrates the Donaldson matrix of a pink sample containing an orange fluorescent color, where a hump in the 600 to 700 nm emission wavelength range represents the luminescent radiance factor of this sample.

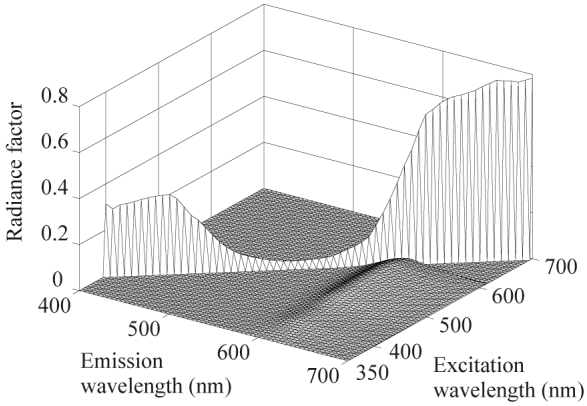

Fig. 1. Donaldson matrix obtained from a pink sample containing an orange fluorescent color.

2.2 Observation model

We consider the matte surface of a fluorescent object without specularity. Let $E(\lambda)$ be the illuminant spectrum of a light source. The spectral radiances observed from the surface under this illuminant are described as a sum of the diffuse reflection component and the luminescent component as follows:

$$\begin{aligned} y(\lambda_{em}) &= S(\lambda_{em})E(\lambda_{em}) + \alpha(\lambda_{em})\int_{350}^{\lambda_{em}} \beta(\lambda_{ex})E(\lambda_{ex})d\lambda_{ex} \\ &= S(\lambda_{em})E(\lambda_{em}) + \alpha(\lambda_{em})C(\lambda_{em}), \end{aligned} \tag{3}$$

where

$$C(\lambda_{em}) = \int_{350}^{\lambda_{em}} \beta(\lambda_{ex})E(\lambda_{ex})d\lambda_{ex}. \tag{4}$$

The spectral observations are also described in a matrix equation. Let **s**, **α**, **e**, and **c** be the N (= 61)-dimensional vectors representing reflectance $S(\lambda)$, emission $\alpha(\lambda)$, and illuminant $E(\lambda)$ in the visible range (400 to 700 nm), and modified excitation $C(\lambda)$, respectively. Then the observations can be summarized in a matrix form as

$$\mathbf{Y} = \mathbf{s}.*\mathbf{e} + \boldsymbol{\alpha}.*\mathbf{c}, \tag{5}$$

where the symbol "$.*$" represents element-wise multiplication.

Suppose that n light sources with different spectral-power distributions are available. When the same fluorescent object surface is illuminated with each of these light sources, the observations can be described as

$$\begin{bmatrix} y_1(\lambda_{em}) \\ y_2(\lambda_{em}) \\ \vdots \\ y_n(\lambda_{em}) \end{bmatrix} = S(\lambda_{em}) \begin{bmatrix} E_1(\lambda_{em}) \\ E_2(\lambda_{em}) \\ \vdots \\ E_n(\lambda_{em}) \end{bmatrix} + \alpha(\lambda_{em}) \begin{bmatrix} C_1(\lambda_{em}) \\ C_2(\lambda_{em}) \\ \vdots \\ C_n(\lambda_{em}) \end{bmatrix} \tag{6}$$

3. Estimation method

For computational simplicity, the observation equation is equivalently described in vector notation as

$$\mathbf{y}(\lambda) = \mathbf{E}(\lambda)S(\lambda) + \mathbf{C}(\lambda)\alpha(\lambda) \tag{7}$$

where n-dimensional column vectors $\mathbf{y}(\lambda)$, $\mathbf{E}(\lambda)$, and $\mathbf{C}(\lambda)$ represent observations, illuminants, and modified excitations at wavelength λ, respectively. The emission spectrum $\alpha(\lambda)$ for a single fluorophore is unimodal, and the effective range is narrow compared with the reflectance spectrum in the visible wavelength range. The emission wavelength range can be roughly predicted in separate ways, such as by use of a UV light source to illuminate the surface. One can also make a prediction via spectral differences between the total reflected radiance factors obtained under two different illuminants. Now let us assume the effective wavelength range for fluorescent emission is (λ_1, λ_2). The visible wavelength range is then partitioned into different wavelength ranges, where (400, λ_1) and (λ_2, 700) consist of only reflection, and the range (λ_1, λ_2) contains both reflection and emission. This wavelength partition makes the estimation procedure effective and simple. The optimal emission range is also determined.

3.1 Estimation of only reflectance

The observations are described simply as

$$\mathbf{y}(\lambda) = \mathbf{E}(\lambda)S(\lambda) \tag{8}$$

where $400 \le \lambda < \lambda_1$ and $\lambda_2 < \lambda \le 700$. In order to minimize the residual error in this range, the least squares estimate of the reflectance radiance factor (surface-spectral reflectance) is obtained in a straightforward manner as

$$\hat{S}(\lambda) = (\mathbf{E}^t(\lambda)\mathbf{y}(\lambda)) / (\mathbf{E}^t(\lambda)\mathbf{E}(\lambda)) \tag{9}$$

where the symbol t represents matrix transposition. The illuminant spectra $E_i(\lambda)$ (i = 1, 2, ..., n) of n light sources were measured using a standard white reference surface with known reflectance and the sensitivity of the spectral imaging system.

3.2 Estimation of both reflectance and emission

In the wavelength range $\lambda_1 \le \lambda \le \lambda_2$, we have

$$\mathbf{y}(\lambda) = \begin{bmatrix} \mathbf{E}(\lambda) & \mathbf{C}(\lambda) \end{bmatrix} \begin{bmatrix} S(\lambda) \\ \alpha(\lambda) \end{bmatrix} \tag{10}$$

The least squares estimate of $S(\lambda)$ and $\alpha(\lambda)$ at each wavelength under n illuminants is obtained as

$$\begin{bmatrix} \hat{S}(\lambda) \\ \hat{\alpha}(\lambda) \end{bmatrix} = \left[\mathbf{X}^t(\lambda)\mathbf{X}(\lambda)\right]^{-1} \mathbf{X}^t(\lambda)\mathbf{y}(\lambda) \tag{11}$$

Optics EXPRESS

where $\mathbf{X}(\lambda)=\left[\mathbf{E}(\lambda) \quad \mathbf{C}(\lambda)\right]$. The modified excitation spectrum $\mathbf{C}(\lambda)$ is calculated as

$$C_i(\lambda)=\sum_{\lambda_{ex}=350}^{\lambda}\beta(\lambda_{ex})E_i(\lambda_{ex}) \tag{12}$$

The excitation spectrum $\beta(\lambda)$ can be estimated using a physical model describing the relationship between the excitation and reflection spectra:

$$\beta(\lambda)=Q(\lambda)(1-\hat{S}(\lambda)), \tag{13}$$

where $Q(\lambda)$ is the luminescence efficiency [18, 19]. The luminescence efficiency was determined by applying Eq. (13) to direct measurements of $\beta(\lambda)$ and $S(\lambda)$ for 12 fluorescent samples from different products, such as sheet, paint, cardboard, and plastic [11]. We obtained the Donaldson matrix for each object with the bispectrometer system. Thin curves in Fig. 2 show the efficiency curves for the respective samples. The curves are normalized with respect to the efficiency value, which to take to be one at 600 nm. Variations in the efficiency curves for different samples appear to be larger at short excitation wavelengths. As wavelength affects the efficiency curves of the samples, the average of these curves was adopted as the luminescence efficiency in this study. In Fig. 2, the average curve for different samples is represented by the bold curve, where the standard deviation curves (+ 1σ and −1σ) were represented by the dotted curves.

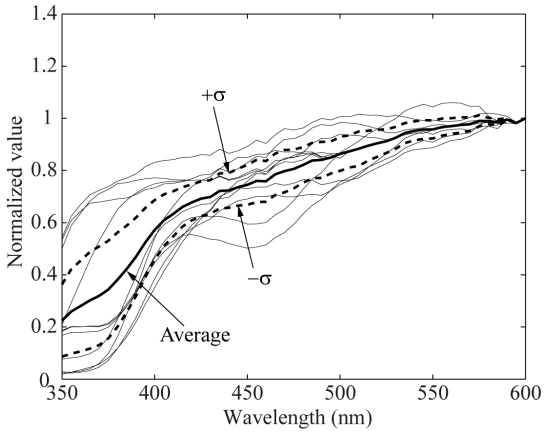

Fig. 2. Luminescent efficiency curve that represents the average curve of the efficiencies for different fluorescent samples. Thin curves represent the efficiencies for 12 different fluorescent objects. The bold curve and the broken curves represent the average curve and the standard deviation curves of $\pm 1\sigma$ from the average, respectively [11].

We note that the reflectance $S(\lambda)$ is nested in Eqs. (11) and (13), thus $S(\lambda)$ and $\alpha(\lambda)$ cannot be determined directly. We adopt an iterative procedure. The initial condition of $\hat{S}(\lambda)$ is set to a constant spectrum in the excitation range. The estimates $\hat{S}(\lambda)$ and $\hat{\alpha}(\lambda)$ are updated using Eqs. (11)-(13) at each iteration step. This procedure is repeated until the residual error $\left\|\mathbf{y}(\lambda)-\hat{\mathbf{y}}(\lambda)\right\|^2$ becomes sufficiently small over the entire wavelength range. Note that the relationship in Eq. (13) is available only for estimation of $\beta(\lambda)$ in $400\le\lambda$ due to observation limitations. The spectral curve of $\beta(\lambda)$ in $350\le\lambda<400$ is estimated by

Optics EXPRESS

interpolation based on the estimates of $\hat{\beta}(\lambda)$ in $400 \le \lambda$ and the terminal condition of $\hat{\beta}(350) = 0$.

3.3 Determination of the emission range

We determine the optimal wavelength range (λ_1, λ_2) for effective fluorescent emission. A pair of (λ_1, λ_2) are two-dimensional variables. We determine the optimal values that minimize the average residual error $J = \overline{\left\| \mathbf{y}(\lambda) - \hat{\mathbf{y}}(\lambda) \right\|^2}$ over the entire visible wavelength range. The emission spectrum $\alpha(\lambda)$ has a single peak as shown in Fig. 3. We judge the unimodal property of $\alpha(\lambda)$ during the estimation procedure. Let λ_p be the peak wavelength of the emission spectrum. It is obvious that the slope of $\alpha(\lambda)$ should be positive when $\lambda_1 \le \lambda < \lambda_p$ and negative when $\lambda_p < \lambda \le \lambda_2$.

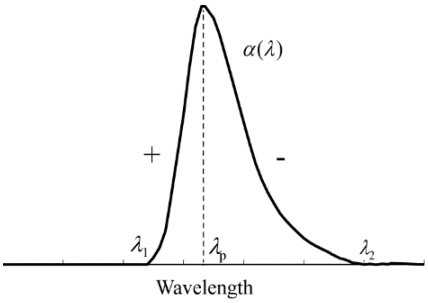

Fig. 3. Unimodality of the emission spectrum.

In Fig. 3, the unimodality was suggested as we had only considered a single fluorescent material in this study. The proposed method only considers a single fluorescent material which could only produce a unimodal emission spectrum. We do not recommend the proposed method for materials with multimodal fluorescence.

4. Experiments

A series of experiments using different fluorescent objects and illuminants was conducted to show the usefulness of the proposed method. The analysis includes precise estimation of the Donaldson matrix, effective selection of illuminants, and application to appearance decomposition and reconstruction. Figure 4 shows the spectral imaging system used in experiments, which consisted of a monochrome CCD camera with 12-bit dynamic range and Peltier cooling (QImaging, Retiga 1300), a VariSpec liquid crystal tunable filter, an IR-cut filter, and a personal computer. Figure 5 shows the total spectral sensitivity functions of the imaging system, including filter transmittances and camera sensitivity. The spectral images were captured at 5 nm intervals in the visible wavelength range, thus each captured image was represented in an array of 61-dimensional vectors. Since the total sensitivities depend on wavelength as shown in Fig. 5, the camera was adjusted so that the captured image intensity was equal in every wavelength channel. Let $R_i(\lambda)$ (i = 1, 2, …, 61) be the spectral sensitivity function of the i-th sensor of the spectral imaging system and T_i (i = 1, 2, …, 61) be the exposure time of the sensor. The exposure time of the camera was determined to satisfy the following relationship for every channel:

$$T_i \int_{400}^{700} R_i(\lambda) d\lambda = const, \qquad (i = 1, 2, \ldots, 61) \tag{14}$$

Optics EXPRESS

Figure 6 shows the spectral-power distributions for the following light sources: (1) an incandescent lamp (Iwasaki, PRF-300W), (2) an artificial sunlight lamp (SERIC, SOLAX 100W), (3) a photographic flood daylight lamp (Iwasaki, PRF-350WD), and (4) a white LED lamp (Hitachi, LDA11D-G/100C). Each illuminant spectral-power distribution was represented in an array of 71-dimensional vectors. Because the light sources used in this study emit unpolarized light, we do not suspect the occurrence of fluorescence polarization. However, since the VariSpec liquid crystal tunable filter is polarization-sensitive, it is possible in principle to sense polarization effects when an object is illuminated with a strong polarized light source.

In this paper, all gathered images and the analysis results are displayed in sRGB color images in order to reproduce accurate color appearance in a calibrated display device. To this end, all spectral images were first transformed into the CIE-XYZ images by using the color-matching functions, and were then converted to the sRGB images.

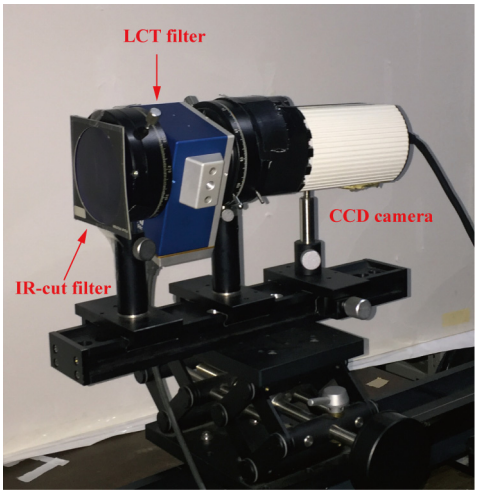

Fig. 4. Spectral imaging system used in experiments.

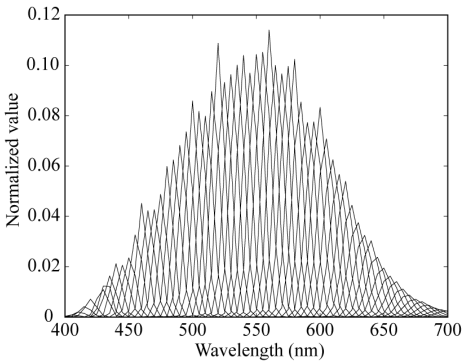

Fig. 5. Total spectral sensitivity functions of the imaging system.

Optics EXPRESS

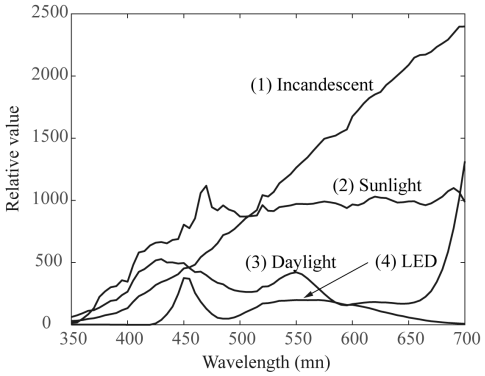

Fig. 6. Illuminant spectral-power distributions of four light sources.

4.1 Estimation accuracy

The test samples were chosen from general objects that one can easily find in daily life. Figure 7 shows the observed images of (a) a pink sample and (b) a green sample under illumination with four different light sources. We made these samples by pasting cut sheets (product name: Lumino Sheet, manufacturer; Okina Inc.) on a board with dimensions of about 5 cm by 5 cm. Unfortunately, the manufacturers of the fluorescent objects did not provide us the details of the fluorescent substances included in the test objects. A portion of these images was used for estimation.

The estimation algorithm was run by iteratively changing the emission wavelength range (λ_1, λ_2) while searching for the minimum average residual error J. The iterative algorithm converged after about three iterations in every case. Figure 8 depicts the average residual error for the pink sample as a function of λ_1 and λ_2. The unimodal property of the emission spectrum was satisfied in this range. Error minimization was achieved with J = 3.5 at λ_1 = 565 nm and λ_2 = 700 nm. Thus, the emission range was determined to be 565 to 700 nm. The estimated spectral curves of reflection, emission, and excitation for the pink sample are depicted in Figs. 9(a)-9(c). It is shown in Figs. 9(a) and 9(b) that the object color of this sample is pink, while the fluorescent color is orange. The Donaldson matrix constructed with the estimated spectral curves is shown previously in Fig. 1.

Next, the estimation results for the green sample are shown in Figs. 10-12. The residual error was minimized with J = 12.9 at λ_1 = 480 nm and λ_2 = 660 nm in Fig. 10, and the emission range was determined to be 480 to 660 nm. The estimated spectral curves in Fig. 11 and the Donaldson matrix in Fig. 12 suggest that the fluorescent material emits more saturated green light than the original green color of the object because the emission range is narrower than the reflectance range.

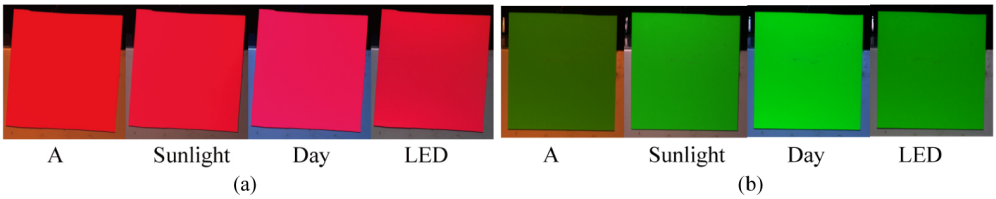

Fig. 7. Observed images of two fluorescent samples of (a) pink and (b) green under four light sources.

Optics EXPRESS

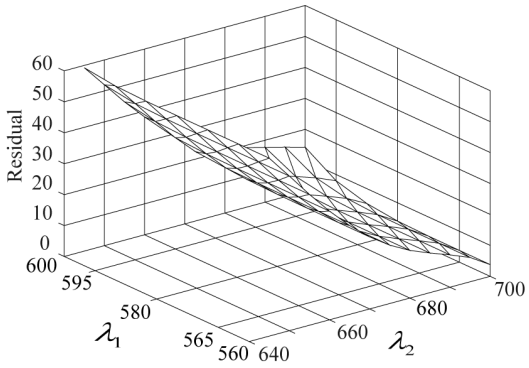

Fig. 8. Average residual error for the pink sample as a function of parameters λ_1 and λ_2.

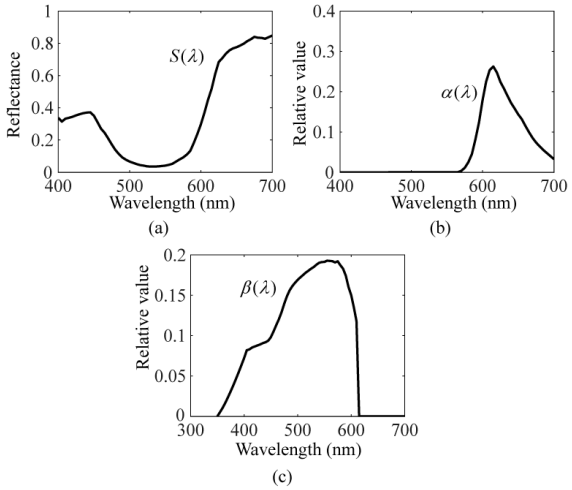

Fig. 9. Estimated spectral curves of (a) reflection, (b) emission, and (c) excitation for the pink sample.

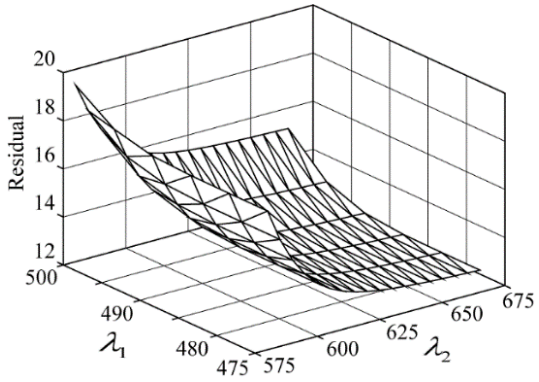

Fig. 10. Average residual error for the green sample as a function of parameters λ_1 and λ_2.

Optics EXPRESS

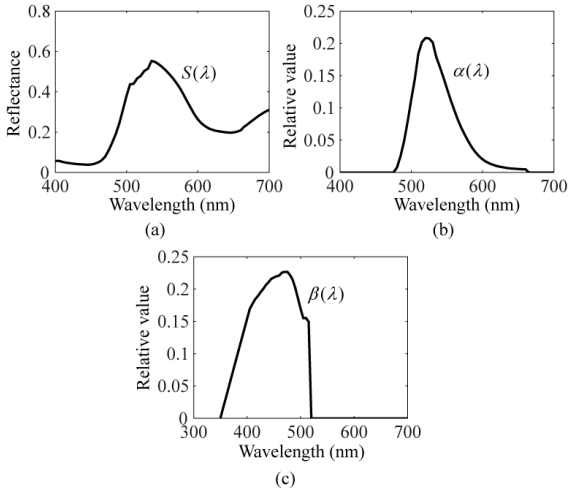

Fig. 11. Estimated spectral curves of (a) reflection, (b) emission, and (c) excitation for the green sample.

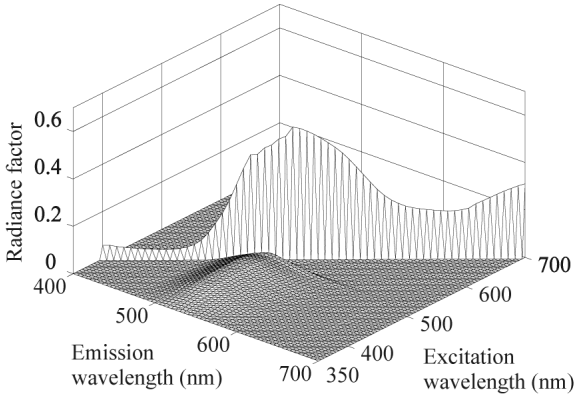

Fig. 12. Estimated Donaldson matrix for the green sample.

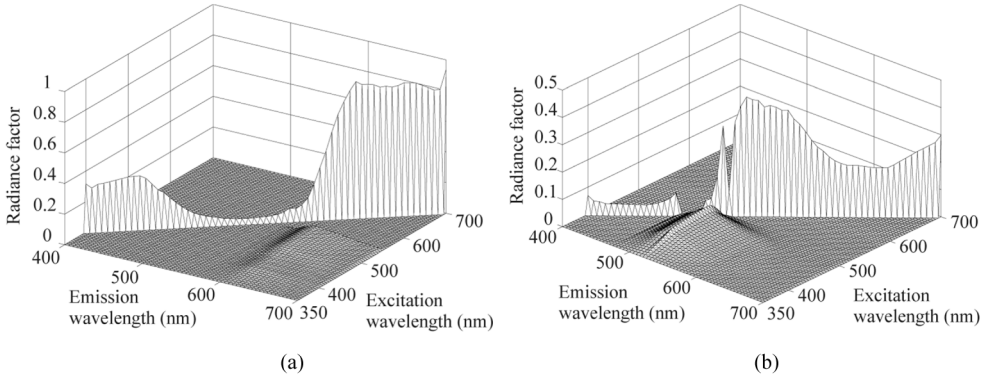

Fig. 13. Donaldson matrices for (a) pink and (b) green samples obtained by the previous method [11], where two light sources (1) and (2) were used to illuminate the same samples.

For comparison, Fig. 13 shows the Donaldson matrices obtained by the previous method in [11], where two light sources (1) and (2) were used to illuminate the same fluorescent samples. The average residual error was $J = 47.3$ and $J = 68.2$ for the pink and green samples,

respectively. These values are much larger than those using the present method. The estimated reflectance curves exhibit an unusual discontinuity, as shown in Fig. 13(b).

4.2 Illuminant selection

We investigated how the illuminant spectra influenced the estimation performance. Since a brighter light source with higher power distribution is more effective for estimating the Donaldson matrix, the illuminants in Fig. 6 were normalized to have the same power. Figure 14 shows a set of illuminant spectral curves with $\|\mathbf{e}_i\| = \text{constant}$ (i = 1, 2, 3, and 4), which were used in a numerical simulation for bispectral estimation. The same estimation algorithm was executed for different illuminant combinations. The performance indices in typical combinations for the pink sample are as follows:

$$J(1,2)=0.075,\ J(2,3)=0.073,\ J(1,3)=0.092,\ J(1,2,3)=0.071,\ J(1,2,3,4)=0.164$$

These results suggest that the use of all of the illuminants does not lead to the best performance. We suggest that by using only two illuminants, i.e., (2) sunlight and (3) daylight, we can produce a result that is close to the best performance $J(1, 2, 3) = 0.071$. The use of (1) incandescent light is less effective. We consider that the illuminant has less spectral energy in the excitation range at UV and blue wavelengths. It is found that the use of (4) LED significantly degrades the performance. This is because the LED illuminant used in the present experiment has large spectral variation and has little spectral energy in the UV and shorter blue wavelengths compared to the other illuminants in Fig. 14. It is obvious that such a LED illuminant is not suitable for use in the present estimation method. We conclude that it is essential for the illuminant to have a certain amount of energy at shorter wavelengths.

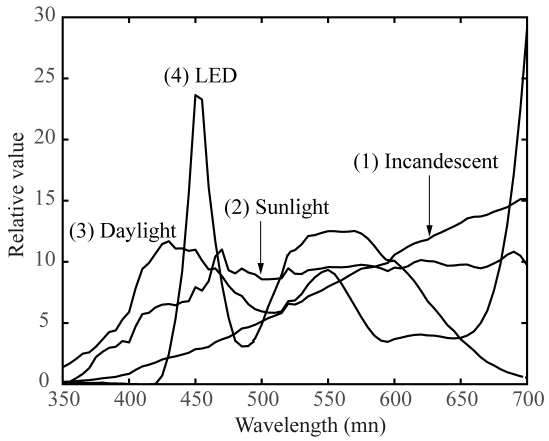

Fig. 14. Illuminant spectral curves normalized to the same power.

4.3 Application to appearance decomposition and reconstruction

Since the proposed method makes estimation of the precise Donaldson matrix at every pixel point in a scene containing different fluorescent objects, we can consider various appearance analyses applied to a fluorescence scene. Since the Donaldson matrix is spectrally constructed with the reflection component and the luminescent component as $\mathbf{D}=\mathbf{D}_R+\mathbf{D}_L$, the image observed with illuminant $\mathbf{e}$ is decomposed into $\mathbf{D}_R\mathbf{e}$ and $\mathbf{D}_L\mathbf{e}$. The appearance of the reflection component depends directly on the illuminant $\mathbf{e}$. Although the intensity depends on the illuminant, the luminescent component always has the same spectral composition as the emission spectrum. We should note that, once we estimate the Donaldson matrices for the

Optics EXPRESS

fluorescent objects, we can spectrally reconstruct the appearance of the same object with an arbitrary illuminant. In other words, we can produce the spectral image required to predict the relighting result of the same object by using an arbitrary illuminant.

Figure 15 shows the observed images of a scene with different objects under illumination with (1) incandescent light and (2) sunlight. The scene contains six pencils, two erasers, and a white plate. The fluorescent pencils were Textsurfer® dry triangular highlighter pencils produced by Steadtler, and the non-fluorescent pencils were Color pencils produced by Tombo. The erasers were Resare produced by Kokuyo. The white plate was a white calibration plate (Konica-Minolta CRA43) made of a glass coated fine ceramic, whose chief ingredient was aluminum (III) oxide (Al_20_3). The Donaldson matrix was estimated at each pixel using the proposed algorithm. Then, the observed images were decomposed into their reflection and luminescent components based on the estimated matrices, as shown in Figs. 16 and 17. It is seen that the objects with fluorescence are clearly separated from the non-fluorescent objects. Figure 17 shows only the fluorescent objects of three pencils and two erasers. The fluorescent objects in Fig. 17 (a) appear darker than the objects in Fig. 17 (b) because the incandescent light has less energy in the shorter wavelength range. Note that the fluorescent colors in Fig. 17 (a) have the same chromaticities as in Fig. 17 (b).

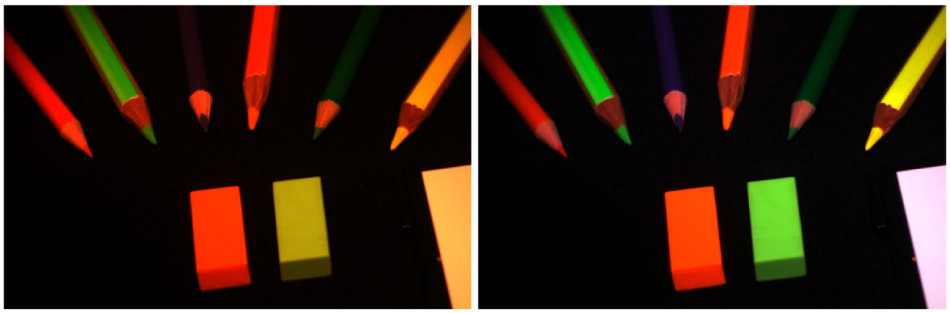

(a) (b)

Fig. 15. Observed images of a scene with different objects under two light sources. ((a): incandescent and (b): sunlight).

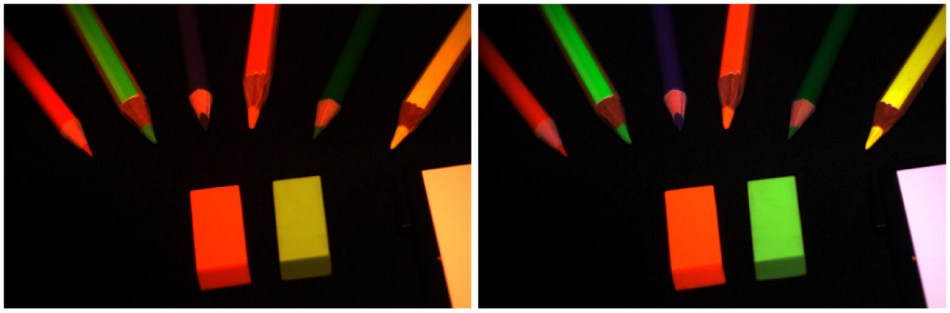

(a) (b)

Fig. 16. Appearance of the reflection component. ((a): incandescent and (b): sunlight).

Optics EXPRESS

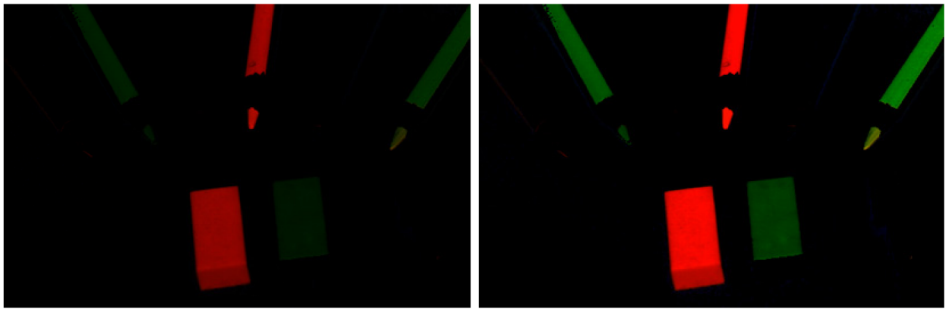

(a) (b)

Fig. 17. Appearance of the luminescent component. ((a): incandescent and (b): sunlight).

We used the illuminant spectral-power distributions of a white LED and a RGB mixing LED shown in Figs. 18(a) and 18(b) for appearance reconstruction. The two light sources have the same color temperature of about 6500 K. Figure 19 demonstrates the appearance reconstruction results of the same scene by illuminating with the two LED lights. The white plates in Figs. 19(a) and 19(b) present the same color appearance under the two illuminants because the sources have the same color temperature. It is interesting to observe that the appearances of the yellow pen and the green pen are distinguishable between the two figures. When Figs. 19(a) and 19(b) are compared, one can see in Fig. 19(a) that the green appears emphasized so that the yellow pen shifts to green and the green pen is saturated, compared with in Fig. 19(b). This is because the white LED illuminant has a much larger amount of shorter wavelength components that contribute to green fluorescent emission. Thus, the appearance of fluorescent objects is strongly affected by the illuminant spectral curve. The proposed method is useful for various purposes including these spectral analysis and spectral reconstruction of a fluorescent object scene.

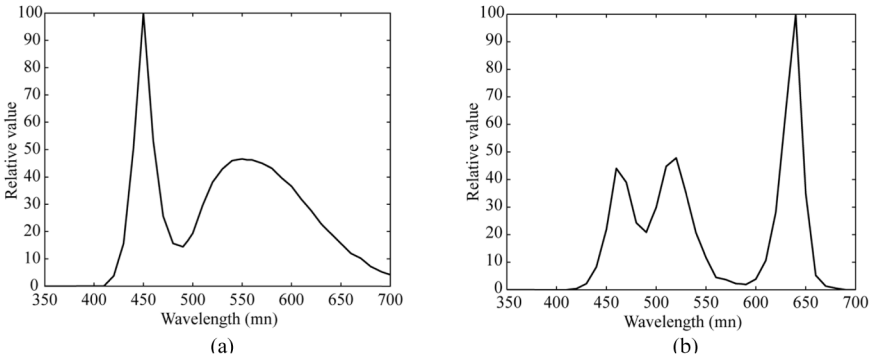

Fig. 18. Illuminant spectral-power distributions of (a) white LED and (b) RGB mixing LED, which have the same color temperature of about 6500 K.

Optics EXPRESS

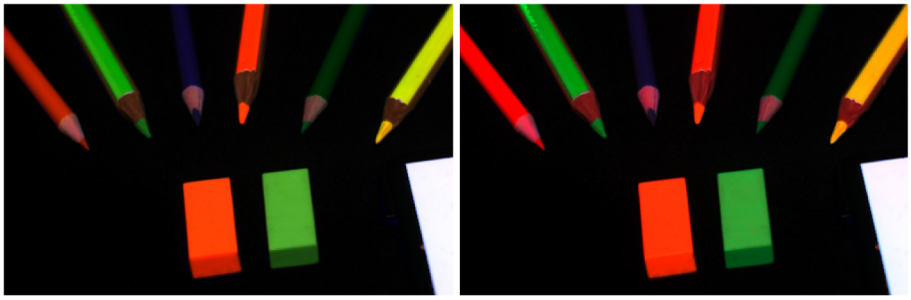

(a) (b)

Fig. 19. Appearance reconstruction results of the same scene by illuminating the two LED lights. ((a): white LED and (b): RGB mixing LED).

4.4 Useful and practical applications

The developed algorithm and multispectral imaging system can have various applications in computer vision, image processing, and computer graphics [20], as well as many other fields including biology, medical diagnosis, food science, material science, and art inspection. In the field of biology, after discovery of green fluorescent protein by Shimomura et al. [21], many studies have been conducted on chlorophyll fluorescence analysis [22]. Fluorescence imaging provides a useful tool to investigate the photosynthetic activities of plant leaves with chlorophyll [23], and to identify plants and characterize their state of health in remote sensing [24].

In medical diagnosis, fluorescence imaging provides an important diagnostic method [25]. For instance, fluorescence spectroscopy of skin shows significant differences between normal and tumorous tissue, both from the point of view of detecting endogenous signals and of using of exogenous fluorescent markers [26]. Combining the multispectral reflection mode imaging with the fluorescence imaging in a single instrument lends strength to the proposed technique. Therefore, if the S/N (signal-to-noise) ratio is high, the proposed technique could be applied to discriminate pathological tissues from normal tissues in biomedicine by using an ordinary light source. Reconstruction may be possible if the fluorescence component of the signal and the intrinsic sample fluorescence are spectrally distinguishable. Since the bispectral characteristics in the proposed technique could be estimated at each pixel point, two-dimensional distribution and visualization of fluorescence is possible.

In food science, the analysis based on an excitation-emission matrix (EEM), called a fluorescent fingerprint, has been successfully applied to quality evaluation of different types of food [27, 28]. In material science applications, bispectral spectrophotometry is used for colorimetry and radiance evaluation of fluorescent printing materials [29, 30]. A similar fluorescent analysis is also used for evaluation of groundwater and wastewater [31]. In art inspection, a noninvasive technique based on fluorescent spectroscopy is used to characterize the painting materials and evaluate the conservation state [15].

The accuracy of the Donaldson matrix estimation depends on the imaging geometry. In this paper, we consider the light source to be located in the vertical direction with respect to the object surface, and the camera in front observes the illuminated surface. Since the object surface is a Lambertian diffuser, the observed signal intensities depend on the incidence angle of light rather than the viewing angle. As the incidence angle increases toward the grazing angle, the reflection and emission signal intensities decrease, leading to decreased estimation accuracy. The accuracy also depends on the curvature of the surface in a similar way. If the surface roughness is low, the estimation results for a rough surface show that the performance is similar to the results from a smooth surface.

Optics EXPRESS

5. Conclusions

In this paper, we have proposed a method to estimate the bispectral Donaldson matrices of fluorescent objects using a spectral imaging system. This is the first attempt to use multiple ordinary light sources where continuous spectral-power distributions were projected sequentially to the object surfaces without controlling the illuminant spectral shape. The problem of estimating the Donaldson matrices was solved as an optimization problem, where the residual error of the observations acquired by the spectral imaging system is minimized. We estimated the spectral functions of reflection, emission, and excitation at each wavelength without using a basis function approximation.

To improve the estimation efficiency, the output visible range was segmented into two wavelength ranges. One consisted only of reflection, and another consisted of both reflection and emission. An iterative estimation algorithm was developed based on this wavelength segmentation and the physical excitation model. The optimal fluorescent emission range was determined based on the error minimization method. We examined the usefulness of the proposed method in experiments using different fluorescent objects and illuminants. We showed the estimation accuracy of the Donaldson matrices, discussed the effective selection of illuminants used, and demonstrated an application to spectral analysis and reconstruction of a fluorescent image.

The proposed method has several useful features. The algorithm obtained here is simple and stable, which is optimized in the sense that the estimates are determined to minimize the residual error of the observations. The Donaldson matrix estimation procedure is more direct and does not require external control over the illuminant spectra, nor does it require a basis approximation of spectral functions. The Donaldson matrices were represented as a spectrally high-dimension 71 × 61 array with an excitation range of 350–700 nm and emission range of 400–700 nm. Because of these useful features, we can easily extend the present method to wider spectral ranges. If the Donald matrices are measured directly by the two-monochromator method, the reliability and accuracy can be verified clearer. Therefore, we suggest that further studies should include a comparison with the direct measurement results of the Donald matrices.

Funding

MEXT (Grant-in-Aid for Scientific Research on Innovative Areas, No. 15H05926).